Z. Phys. B – Condensed Matter 77, 497–510 (1989)

Condensed
Zeitschrift für Physik B Matter

© Springer-Verlag 1989

The effect of measurement on the quantum features of a chaotic system

B.C. Sanders* and G.J. Milburn
Department of Physics, University of Queensland, St. Lucia, Queensland, Australia

Received March 29, 1989

We investigate the quantum dynamics of a periodically kicked nonlinear spin system which exhibits regular and chaotic dynamics in the classical regime. The quantum behaviour is characterised by the evolving eigenvalue distributions for the angular momentum components and the features, including recurrences in the quantum means and the presence of quantum tunneling, are discussed. We employ the evolution operator eigenvalue distribution to prove that coherent quantum tunneling occurs between the fixed points in the regular regions of phase space. Continual quantum measurement is included in the model: the classical dynamics are unchanged but a destruction of coherences occurs in the quantum system. Recurrences in the means are destroyed and quantum tunneling is suppressed by measurement, a manifestation of the quantum Zeno effect.

1. Introduction

In a series of recent papers the dynamics of a spin system which, in its classical form, exhibits both regular and chaotic dynamics has been investigated [1–5]. The model describes the dynamics of an angular momentum vector **J** moving, with J^2 conservation, in a linear precessional motion about one direction and subjected to impulsive nonlinear precessional kicks about an orthogonal direction. Quantum mechanically the system is described in terms of a finite dimensional Hilbert space of dimension $2j+1$ where $j(j+1)$ is the J^2 eigenvalue, and thus no truncation scheme is required. This is one of the most desirable aspects of the model. The Hamiltonian was chosen so as to allow for classically chaotic behaviour as $j \to \infty$.

Quantum mechanically the model is completely integrable in the sense that the dynamics is completely determined by the diagonalisation of a $2j+1$ unitary matrix which determines the evolution of the initial quantum state. As the spectrum of the evolution matrix is discrete all quantum expectation values behave quasiperiodically [2]. The initial states chosen for the quantum analyses are the spin coherent states. As these states are minimum uncertainty states well localised on the sphere as $j \to \infty$ they provide an excellent set of states for investigating the dynamics in the semiclassical limit ($j \to \infty$).

Classically the dynamics may be reduced to an effective two-dimensional nonlinear map of points on the unit sphere. The model exhibits a fascinating set of symmetries which greatly facilitate the search for fixed points and the nature of periodic orbits. In the parameter range of interest to us, hyperbolic fixed points and elliptic fixed points of period one, two and four coexist with regions of chaotic behaviour.

Haake et al. [2] showed that if the initial state was chosen to be localised in the vicinity of the period one fixed point, i.e. in the region of regular dynamics, the mean of the y-component of angular momentum initially exhibited damped oscillations. This corresponds classically to the shearing of an initial density of points about the period one fixed point, and for short times $\sim \ln j$ the classical and quantum moments were indistinguishable. For longer times, ($\sim j$), however, the quantum means recur to values arbitrarily close to the initial value. In fact in the regular region these recurrences occur as well-defined "revivals" of the initial oscillations separated by quiescent periods during which the quantum mean remains close to the classical steady state value. The picture is quite

* *Present address:* Department of Physics, University of Waikato, Hamilton, New Zealand

different for an initial state localised in the chaotic region of the classical map. Recurrences of the quantum means still occur but are now irregular and do not exhibit the well-defined collapse and revival sequence of the regular region. Thus recurrences, either regular or irregular, are a characteristic quantum feature of this system and represent a dramatic departure of the quantum dynamics from that expected classically. Collapse and revival sequences are characteristic of the quantum dynamics of a number of nonlinear systems [6]. Haake et al. conclude that "classical chaos can therefore live in quantum expectation values as a transient only".

In more recent work Grobe and Haake [4, 5] discuss another characteristic quantum feature of this model which is manifest on much larger time scales and can be described as coherent quantum tunneling between fixed points. We believe this to be the first identification of such a phenomenon. This effect is completely analgous to the coherent oscillations between the two wells of a bistable potential for a state initially localised in one well. However the structure in the case of the dynamics of the kicked top is complicated by the fact that it is two dimensional, the motion around each "well" is highly nonlinear and the "wells" or fixed points are separated by regions of chaoticity.

Our first purpose in this paper is to give a more complete characterisation of this complicated tunneling process and indeed to provide conclusive evidence that it can be correctly viewed as coherent tunneling between fixed points. We extend the discussion of Grobe et al. which concerned only the period two fixed point to include the period one fixed point and a regular point near the period one fixed point.

As indicated above the model of Haake and coworkers exhibits two characteristic quantum features, recurrences and coherent tunneling, which cause a departure of the quantum and classical dynamics. Our second purpose is to determine the effect on these quantum features of continual observation of the system. A theory to describe the dynamics of a system subject to continual (repeated) observation of one of the system variables (say J_z in our case) has been in place for a number of years [7–9] and we will use these results here. Essentially the effect of observation is accounted for by including in the evolution of the system an irreversible diffusive term proportional to one parameter Γ. This parameter is itself defined as the quotient of the bandwidth of the continual observation and the accuracy of the observation.

Grobe and Haake [4, 5] have considered the effects of weak dissipation on the quantum features of this model and as we will show the effect of continual observation is similar. The measurement does not modify the classical dynamics but alters the quantum behaviour. In particular quantum tunneling is suppressed more effectively as j increases.

We also consider the so-called "quantum Zeno effect" in the model. This refers to the considerable disruption of the free dynamics of a system with a discrete spectrum subject to combined repeated observation on a time scale much faster than the time scales characterising the reversible dynamics.

In section two we briefly describe in more detail the classical and quantum features of Haake's model. We discuss the features of quantum recurrence and, more extensively, quantum tunneling in Sect. 3. As we will show the picture of quantum tunneling is quite complicated, but we provide conclusive evidence that the phenomenon is correctly identified. In section four we introduce the theory of continual observation and determine its effect on the quantum features of our nonlinear model.

2. The kicked nonlinear top

The states of a classical spinning top are represented by the angular momentum variable **J** in three-dimensional space. The dynamic evolution of the top corresponds to the motion of the **J** vectors in the phase space. The top which we consider undergoes a nonlinear precession around the z-axis and is interrupted by periodic linear impulses, or kicks, around the y-axis. The classical Hamiltonian is

$$H=\frac{\kappa J_z^2}{2j\tau}+pJ_y\sum_{n=-\infty}^{\infty}\delta(t-n\tau) \tag{2.1}$$

for τ the duration between kicks and $j=(\mathbf{J}\cdot\mathbf{J})^{1/2}$ a constant. The phase space is restricted to the sphere of radius j and the angular momentum vector can be parametrized in polar coordinates as

$$\mathbf{J}=(j\sin\theta\cos\varphi, j\sin\theta\sin\varphi, j\cos\theta). \tag{2.2}$$

The constants κ and p in (2.1) are chosen to produce the desired balance of regular and chaotic dynamics.

We investigate the stroboscopic evolution of the top at the times immediately preceding the kicks. The dynamics are identical to the stroboscopic evolution of the model investigated by Haake et al. [1–3]

$$H=\frac{p}{\tau}J_y+\frac{\kappa}{2j}J_z^2\sum_{n=-\infty}^{\infty}\delta(t-n\tau) \tag{2.3}$$

at times immediately subsequent to the J_z^2 kick. The model (2.1) is preferred here as a continuous measurement of J_z is included in Sect. 4 which is concurrent

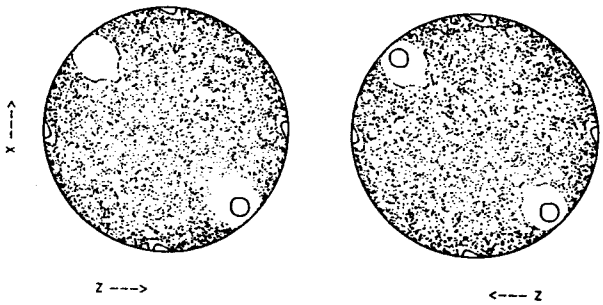

Fig. 1. The stroboscopic phase space dynamics of the classical kicked nonlinear top for $p=\pi/2$ and $\kappa=3$. The trajectories are constrained to the unit sphere. The northern hemisphere ($Y\geqq 0$) and the southern hemisphere ($Y\leqq 0$) are projected onto the $X-Z$ plane and a right-handed orientation of the X, Y, Z axes is maintained. Seventy-five initial points in the northern hemisphere and the 75 R_x-image of the initial points have been randomly selected. The stroboscopic trajectories of these 150 points have been plotted, each for a duration of 133 kicks

with the nonlinear precession about the z-axis. A detailed analysis of the nonlinear rotator without kicks, which corresponds to the case where $\kappa=0$, has been performed [10] and provides insight into the dynamics of the top between kicks.

We review the classical dynamics, as given by Haake et al. [2], for the special case that $p=\frac{\pi}{2}$. The classical stroboscopic dynamics of the normalized angular momentum variable $\mathbf{X}=\mathbf{J}/j$ are determined from the recursive formula

$$\mathbf{X}'=F(\mathbf{X})=\begin{bmatrix} Z\cos kX+Y\sin kX \\ -Z\sin kX+Y\cos kX \\ -X \end{bmatrix}. \tag{2.4}$$

The map possesses the two important symmetries

$$FR_x=R_xFR_y \quad \text{and} \quad FR_y=R_yF; \tag{2.5}$$

here R_x and R_y define rotations of π about the x and y axes, respectively. Thus, F is invariant under R_y and F^2 is invariant under R_x.

Henceforth $\kappa=3$ is assumed. The dynamics of the top are shown in Fig. 1 where the two disks are projections of the unit sphere onto the $X-Z$ plane and a right-handed orientation of the axes is maintained. The points on the sphere are the values of $\mathbf{X}$ for numerous trajectories of finite duration. The initial point is then mapped by R_x onto the other hemisphere and the trajectory is plotted. Elliptic fixed points are evident in the northern hemisphere ($Y\geqq 0$) and a southern two-cycle is apparent. Furthermore an equatorial four-cycle and a large chaotic region exist. There are unstable fixed points at the poles ($Y=\pm 1$) which are not apparent in Fig. 1.

The Hamiltonian for the quantum top is given by (2.1) where $\mathbf{J}$ is the angular momentum operator such that ($\hbar=1$)

$$[J_i, J_j]=i\sum_k \varepsilon_{ijk}J_k. \tag{2.6}$$

The Casimir operator $\mathbf{J}\cdot\mathbf{J}$ commutes with H and $j(j+1)$ is the eigenvalue for j an integer. For given j the Hilbert space is $(2j+1)$-dimensional and the orthonormal J_z-eigenstates $\{|jm\rangle: -j\leqq m\leqq j\}$, such that $J_z|jm\rangle=m|jm\rangle$, are the standard basis.

The quantum analog to the iterative map (2.4) is the evolution operator

$$U=\exp\left\{-\mathrm{i}\frac{\kappa}{2j}J_z^2\right\}\exp\left\{-\mathrm{i}\frac{\pi}{2}J_y\right\}. \tag{2.7}$$

The orthonormal eigenstates of U, denoted by $\{|\phi_m\rangle: -j\leqq m\leqq j\}$, which satisfy

$$U|\phi_m\rangle=\exp(\mathrm{i}\phi_m)|\phi_m\rangle, \tag{2.8}$$

provide a convenient basis for studying the stroboscopic evolution. An arbitrary state

$$|\psi\rangle=\sum_{m=-j}^{j}|\phi_m\rangle\langle\phi_m|\psi\rangle \tag{2.9}$$

evolves to

$$U^n|\psi\rangle=\sum\exp(\mathrm{i}n\phi_m)|\phi_m\rangle\langle\phi_m|\psi\rangle \tag{2.10}$$

just prior to the kick at time $n\tau$. The analogues of the classical symmetries (2.5) are

$$UR_x=R_xUR_y \quad \text{and} \quad UR_y=R_yU \tag{2.11}$$

where R_x and R_y are unitary operators defining rotations of π about the x and y axes, respectively. As R_y commutes with U and $R_y^2=1$, the states $\{|\phi_m\rangle\}$ are even or odd parity under R_y:

$$R_y|\phi_m^{\pm}\rangle=\pm|\phi_m^{\pm}\rangle. \tag{2.12}$$

As $\mathrm{tr}(R_y)=(-1)^j$ and as the trace is invariant under a change of basis it follows that, for j even, there are $j+1$ even eigenstates and j odd states while, for j odd, there are j even eigenstates of U and $j+1$ odd states. It follows from (2.11) that

$$U(R_x|\phi_m^{\pm}\rangle)=\pm\exp(\mathrm{i}\phi_m)(R_x|\phi_m^{\pm}\rangle). \tag{2.13}$$

For the odd states,

$$R_x|\phi_m^{-}\rangle=\pm|\phi_m^{-}+\pi\rangle; \tag{2.14}$$

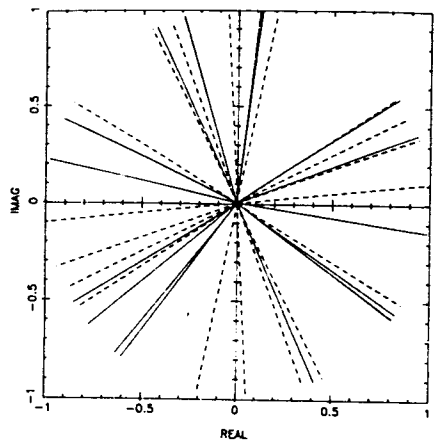

Fig. 2. A phasor diagram of the eigenphases for $j=18$. Each eigenvector of U, $|\phi_m\rangle$, is associated with an eigenvalue $\exp(i\phi_m)$, which is plotted as a unit vector. If the eigenvector is even (odd) the unit vector is a solid (dash) line. Some eigenphases are degenerate. For each odd eigenphase ϕ, there exists an odd eigenphase $\phi+\pi$

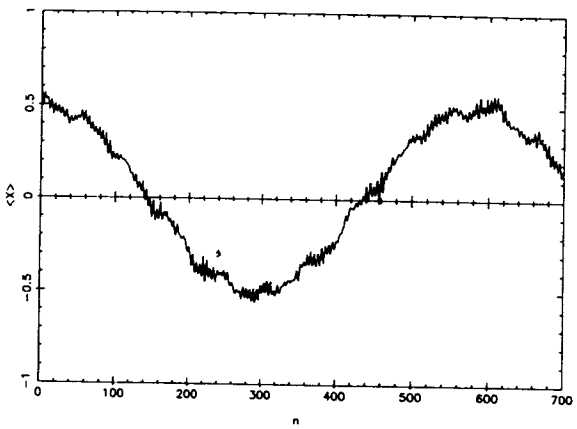

Fig.3. The quantum mean $\langle X\rangle$ for the initial coherent state $|F\rangle$ which has a mean at an elliptic fixed point

each odd state $|\phi_m^-\rangle$ is paired with an odd state $|\phi_m^- + \pi\rangle$ with eigenvalue $-e^{i\phi_m}$. Each odd pair is even or odd under R_x. For the even states either $|\phi_m^+\rangle$ and $R_x|\phi_m^+\rangle$ are doubly degenerate or

$$R_x|\phi_m^+\rangle = \pm|\phi_m^+\rangle, \tag{2.15}$$

that is, linearly dependent.

The eigenphase distribution for $j=18$ is shown in a phasor diagram (Fig. 2). Even and odd parity eigenstates under R_y are distinguished by solid and dash lines, respectively, and the angle between the vector and the real axis is the eigenphase ϕ_m. The pairing of odd states which are separated by a phase of π and the broad distribution of eigenphases for $j=18$ are evident in Fig. 2.

As an initial condition we follow Haake et al. [2] and take the top to be in a coherent state $|j, \theta, \varphi\rangle$ [11]. These states, which are minimum uncertainty states with respect to the angular momentum operators, are generated from the Dicke state $|jj\rangle$

$$|j, \theta, \varphi\rangle = R(\theta, \varphi)\,|jj\rangle \tag{2.16}$$

by the unitary rotation operator

$$R(\theta, \varphi) = \exp\{-i\theta[J_x \sin\varphi - J_y \cos\varphi]\}. \tag{2.17}$$

The mean of $\mathbf{X} \equiv \mathbf{J}/j$ is

$$\langle j, \theta, \varphi|\,\mathbf{X}\,|j, \theta, \varphi\rangle = (\sin\theta\cos\varphi, \sin\theta\sin\varphi, \cos\theta). \tag{2.18}$$

In Sect. 3 the quantum features of the model are discussed. For the state

$$|F\rangle \equiv |j=18, \theta=2.25, \varphi=0.63\rangle, \tag{2.19}$$

which has a mean at an elliptic fixed point, long timescale oscillations in the mean $\langle X\rangle$ are evident (Fig. 3). As

$$Z = -U^\dagger X U, \tag{2.20}$$

the mean $\langle Z\rangle$ also exhibits oscillations. Such oscillations are nonclassical, as are the quasiperiodic recurrences in $\langle Y\rangle$, which are not shown here [2].

3. Quantum features

The tunneling of a state through a classically impenetrable barrier is a purely quantum phenomenon and has generated much interest [12]. Of particular concern is the case of two finite regions, or wells, of equal energy separated by a finite potential barrier. The state oscillates between the two wells via coherent tunneling. The bistable well illustrates the case of coherent quantum tunneling, The Hamiltonian is given by

$$H = p^2 + (q+a)^2(q-a)^2 \tag{3.1}$$

for p the momentum, q the position and $\pm$ a are the positions of the potential energy lower bounds. The Hamiltonian is invariant under the parity transformation $q \to -q$; thus, the energy eigenstates are either even or odd with respect to q.

The ground state $|\psi_0\rangle$ and the first excited state $|\psi_1\rangle$ have even and odd parity, respectively. The simplest pair of states localized in each well are given by symmetric and antisymmetric combinations of $|\psi_0\rangle$ and $|\psi_1\rangle$. In the Schrödinger picture these states evolve as

$$\begin{aligned}&|\psi_\pm(t)\rangle\\ &= 2^{-1/2}[\exp\{iE_0 t/\hbar\}\,|\psi_0\rangle \pm \exp\{iE_1 t/\hbar\}\,|\psi_1\rangle]\\ &= 2^{-1/2} e^{i\Omega t}[e^{i\epsilon t}|\psi_0\rangle \pm e^{-i\epsilon t}|\psi_1\rangle]\end{aligned} \tag{3.2}$$

for Ω the mean frequency

$$\Omega=[E_0+E_1]/2\hbar \tag{3.3}$$

and ε the half-frequency difference

$$\varepsilon=[E_0-E_1]/2\hbar. \tag{3.4}$$

After a time $t=\pi/2\varepsilon$ a system prepared in a state $|\psi_+\rangle$ evolves to $|\psi_-\rangle$; i.e. a state localized in one well has tunneled through the barrier to be localized in the other well. The distribution $|\langle q|\psi_\pm\rangle|^2$ at $t=\pi/2\varepsilon$ is the mirror image of $|\langle q|\psi_\pm\rangle|^2$ at $t=0$.

The state oscillates coherently between the two wells with a tunneling period $\pi/2\varepsilon$. At half the tunneling period the state formed is a coherent superposition of the two localised states. The position distribution at this time is double-peaked while the momentum distribution exhibits interference fringes. A localized state which consists of more than two energy-eigenstates produces a more complex tunneling behaviour. If the eigenphases are commensurate, the state recurs over a finite time.

The example of the bistable well provides insight for analyzing the kicked nonlinear top. The stroboscopic evolution precludes the use of energy eigenstates; however, the U-eigenstates discussed in Sect. 2 can be used to study the evolution. A similar symmetry argument can be used to estimate the tunneling time as the U-eigenstates are partitioned into even and odd parity states under R_y just as the bistable well states are partitioned under q-parity.

Coherent tunneling between fixed points is suggested by the sinusoidal modulation of $\langle X\rangle$ in Fig. 3. The long time scale oscillation observed here is similar to the two-cycle oscillation in the southern hemisphere observed by Grobe and Haake [4] and is reviewed below. As an illustration of tunneling we consider the bistable well for which the distribution $|\langle q|\psi\rangle|^2$ tunnels from one well to the other in the bistable well and fringe patterns arise in the conjugate distribution $|\langle p|\psi\rangle|^2$. The analogue to the q- and p-distributions for the top are the probability distribution for the components of angular momentum in the direction of the unit vector $\mathbf{n}=(\sin\theta\cos\varphi,\ \sin\theta\sin\varphi,\ \cos\theta)$. That is, the probability distribution for the operator $J_{\mathbf{n}}\equiv\mathbf{J}\cdot\mathbf{n}$ and the state $|\psi\rangle$ is $|{}_{\mathbf{n}}\langle jm|\psi\rangle|^2$ where $|jm\rangle_{\mathbf{n}}$ is an eigenstate of $J_{\mathbf{n}}$ with eigenvalue m. The important eigenvalue probability distributions of the kicked nonlinear top correspond to the operators J_y and

$$J_{\perp,\parallel}\equiv 2^{-1/2}[J_z\pm J_x] \tag{3.6}$$

for $J_\perp$ the component of $\mathbf{J}$ in a direction perpendicular to the line $Z=-X$ and $J_\parallel$ is the component parallel to $Z=-X$. If tunneling does occur between the fixed points on the line $Z=-X$, then the distribution for $J_\parallel$ is analogous to the q-distribution in the double well and $J_\perp$ is analogous to the p-distribution.

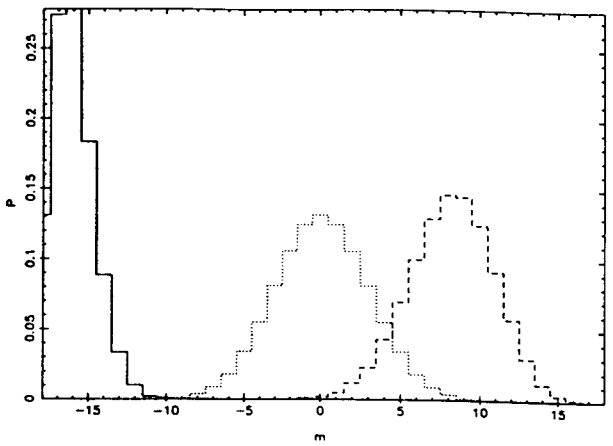

Fig. 4. The $J_\parallel$ (solid line), $J_\perp$ (dotted line) and J_y (dash line) eigenvalue distributions for the coherent state $|F\rangle$

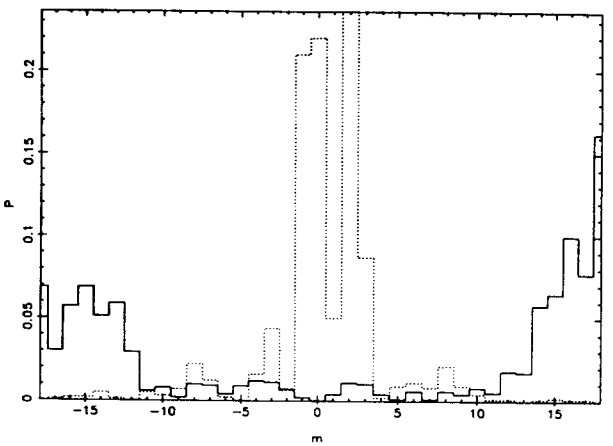

Fig. 5. The $J_\parallel$ (solid line) and $J_\perp$ (dotted line) eigenvalue distribution for the state $U^{150}|F\rangle$

The J_y and $J_{\perp,\parallel}$ eigenvalue distributions for the state $|F\rangle$ are shown in Fig. 4. The means of the distributions are localized about the fixed point (3.5). The variances in the distributions satisfy the minimum uncertainty equalities for the $SU(2)$ algebra. The distributions for $U^n|F\rangle$, where n is small compared to the tunneling time, distorts the J_y and $J_{\perp,\parallel}$ distributions, but the distributions remain localized about the fixed point. The distortion of the distributions leads to the small fluctuations observed for the time-dependent means in Fig. 3. However, the distributions remain localised about the fixed point for the short time scale.

The $J_{\parallel,\perp}$ eigenvalue distributions for the state $U^{150}|F\rangle$ are shown in Fig. 5. For $n=150$, $\langle X\rangle=0$

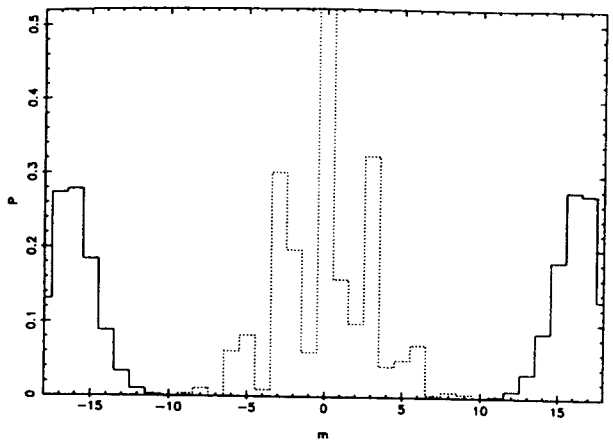

Fig. 6. The $J_{\parallel}$ (solid line) and $J_{\perp}$ (dotted line) eigenvalue distribution for the superposition state $|F^{-}\rangle$

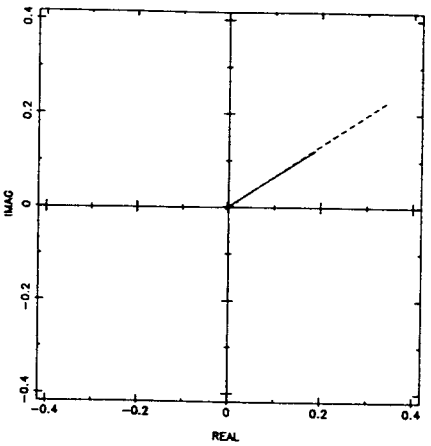

Fig. 8. The probability distribution $|\langle\phi_m|F\rangle|^2$ vs the eigenphase ϕ_m. Solid (dash) lines correspond to the probabilities of even (odd) eigenvectors

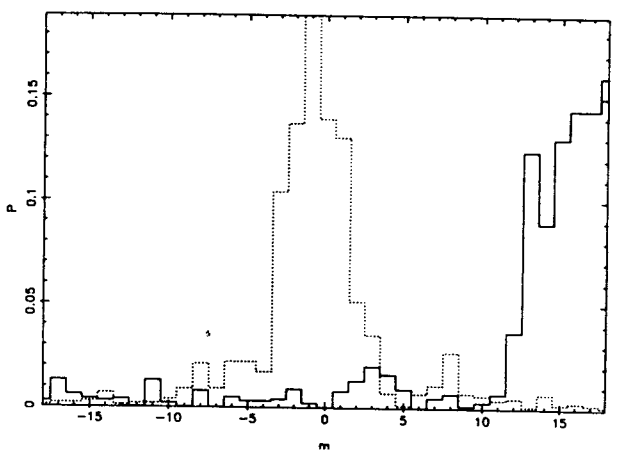

Fig. 7. The $J_{\parallel}$ (solid line) and $J_{\perp}$ (dash line) eigenvalue distribution for the state $U^{300}|F\rangle$

and the bimodal $J_{\parallel}$ eigenvalue distribution and the interference fringes in the $J_{\perp}$ distribution in Fig. 5 suggests that a superposition of the two fixed point states, $|F\rangle$ and $R_y|F\rangle$, has formed. This is confirmed by an inspection of the same eigenvalue distributions for the superposition state

$$|F^{-}\rangle \equiv 2^{-1/2}[e^{i\pi/4}|F\rangle - e^{-i\pi/4}R_y|F\rangle]$$

shown in Fig. 6. Moreover the eigenvalue distribution for $J_{\perp}$ displays "interference fringes" for both $U^{150}|F\rangle$ (Fig. 5) and the superposition state (Fig. 6). This behaviour strongly suggests that quantum tunneling is occurring.

The $J_{\parallel,\perp}$ eigenvalue distributions for $U^{300}|F\rangle$ are shown in Fig. 7. The distributions are now localized about the fixed point at $-X=Z>0$. We conclude that at this time the state has completely tunneled to the opposite fixed point. The J_y eigenvalue distributions for $U^{150}|F\rangle$ and $U^{300}|F\rangle$ are not shown but are localised in the northern hemisphere; thus the tunneling is occurring between the two fixed points.

To further elucidate the nature of tunneling we now consider the probability distribution for the state $|F\rangle$ in the U-eigenbasis. The probability associated with the eigenstate $|\phi_m\rangle$ is given by $|\langle\phi_m|F\rangle|^2$. The probability distribution is plotted as a phasor diagram by plotting the probabilities as vectors for which the magnitude is $|\langle\phi_m|F\rangle|^2$ and the phase of the eigenvector $|\phi_m\rangle$ is ϕ_m. Thus a probability distribution of the various eigenphases is constructed. The probability vectors of even states under R_y rotations are represented as solid lines and dash lines are used to represent the probability vectors for odd states under R_y rotations.

The probability distribution for $|F\rangle$ is presented in Fig. 8. The probability distribution in Fig. 8 is identical to the distribution for both $R_y|F\rangle$ and $U^n|F\rangle$ as well. The state $|F\rangle$ is dominated by one odd vector and two even vectors. The two even vectors have a degenerate eigenphase and the probabilities of the two even eigenvectors are equal for $|F\rangle$. The magnitude of the even vector in Fig. 8 is equal to the probability of *each* even vector. The eigenphases of the dominant odd eigenvector and the degenerate even eigenvector pair are nearly degenerate.

The state $|\phi_m\rangle$ is an eigenstate of U. More generally the state $\exp(i\theta_m)|\phi_m\rangle$ is an eigenstate of U with eigenphase ϕ_m. For each eigenstate $|\phi_m\rangle$ we have the freedom to choose θ_m. For our analysis of $|F\rangle$ we assume that θ_m is chosen such that $\langle\phi_m|F\rangle$ is real and nonnegative for all m and designate these U-ei-

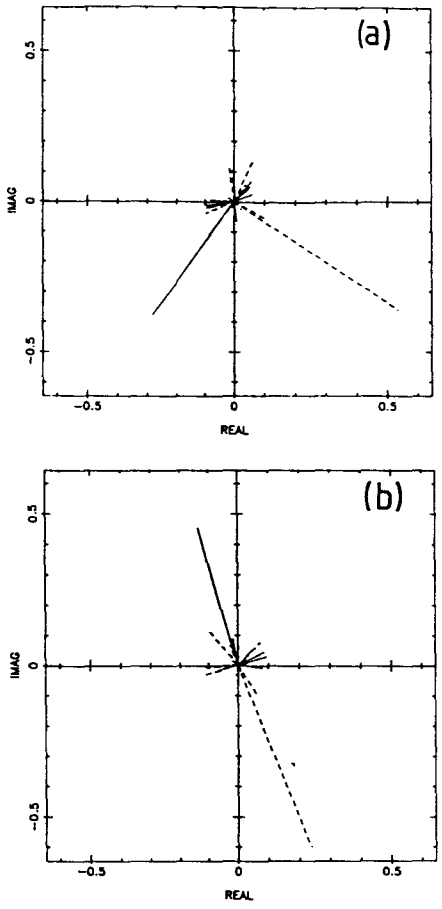

Fig. 9a and b. The complex matrix elements ${}_F\langle\phi_m|U^m|F\rangle$ for **a** $n=150$ and **b** $n=300$

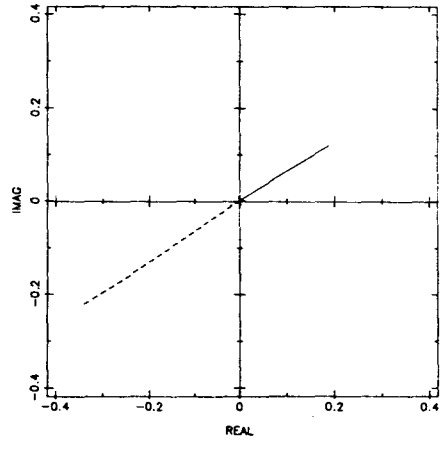

Fig. 10. The probability distribution $|\langle\phi_m|R_x|F\rangle|^2$ vs the eigenphase ϕ_m

genstates as $|\phi_m\rangle_F$. Thus, the matrix elements for the rotated coherent state $R_y|F\rangle$, whose mean is at the other period one fixed point, are also real. However, the matrix element ${}_F\langle\phi_m|R_y|F\rangle$ is nonnegative for $|\phi_m\rangle_F$ even under an R_y rotation and is nonpositive for $|\phi_m\rangle_F$ odd. For the superposition state $|F^-\rangle$, defined in (3.6), the matrix elements are given by the imaginary quantity

$${}_F\langle\phi_m^+|F^-\rangle = i\,{}_F\langle\phi_m^+|F\rangle$$

for even matrix elements and by the nonnegative real quantity

$${}_F\langle\phi_m^-|F^-\rangle = {}_F\langle\phi_m^-|F\rangle$$

for odd matrix elements. The orientation of even and odd matrix elements for $|F\rangle$, $|F^-\rangle$ and $R_y|F\rangle$ are important for the following analysis of tunneling.

In Fig. 9 the matrix elements ${}_F\langle\phi_m|U^n|F\rangle$ are shown for $n=150$ and $n=300$. The predominant odd vector is separated from the predominant even pair by $\pi/2$ and by π for $n=300$. If the matrix elements ${}_F\langle\phi_m|F^-\rangle$ and ${}_F\langle\phi_m|R_y|F\rangle$ were plotted, one would observe that even vectors are coaligned and odd vectors are coaligned; the separation between the even and odd vectors is $\pi/2$ and π, respectively. Thus, the similarity between $U^{150}|F\rangle$ and $|F^-\rangle$ and the similarity between $U^{300}|F\rangle$ and $R_y|F\rangle$ is clear. Furthermore it is clear that the small phase difference between the eigenphase of the dominant odd eigenstate and the dominant doubly degenerate even eigenstate will determine the tunneling frequency. If this phase difference is 2ε, the tunneling period is $N=\pi/2\varepsilon$. The smaller contributing matrix elements ${}_F\langle\phi_m|U^n|F\rangle$ are responsible for the differences between the $J_{\parallel,\perp}$ eigenvalue distributions of $U^n|F\rangle$ and a superposition of $|F\rangle$ and $R_y|F\rangle$.

The U-eigenstate probability distribution provides a valuable tool for determining the evolution of a state. For example the probability distribution for the coherent state $R_x|F\rangle$, which has a mean at a southern two-cycle, is presented in Fig. 10. The dominant even and odd eigenphases are separated by 2ε in Fig. 8; in Fig. 10 we observe that the dominant even and odd eigenphases for $R_x|F\rangle$ are separated by $\pi+2\varepsilon$. In addition to the tunneling period of $\pi/2\varepsilon$, the state undergoes the two-cycle behaviour

$$U^{2n+1}[R_x|F\rangle] = R_x[U^{2n+1}R_y|F\rangle] \tag{3.7a}$$

and

$$U^{2n}[R_x|F\rangle] = R_x[U^{2n}|F\rangle] \tag{3.7b}$$

as required by (2.11).

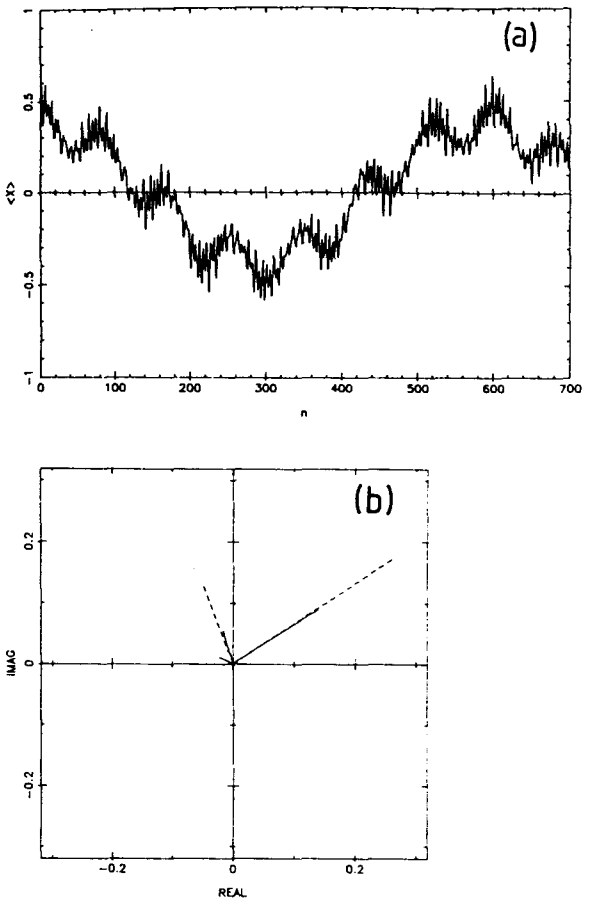

Fig. 11a and b. The quantum mean a $\langle X \rangle$ for the initial coherent state $|P\rangle$ and b the probability distribution $|\langle \phi_m | P \rangle|^2$ vs ϕ_m

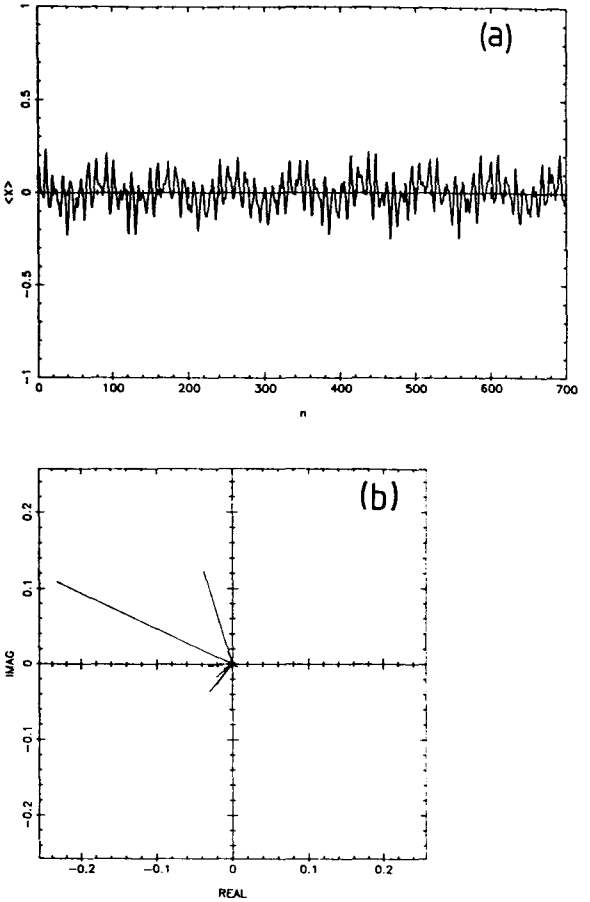

Fig. 12 a and b. The quantum mean a $\langle X \rangle$ for the initial coherent state $|C\rangle$ and b the probability distribution $|\langle \phi_m | C \rangle|^2$ vs ϕ_m

In Fig. 11a we view the mean $\langle X \rangle$ for the state

$$|P\rangle \equiv |j=18, \theta=2.10, \varphi=0.94\rangle \tag{3.8}$$

which has a mean in the stable region near an elliptic fixed point. The mean $\langle Z \rangle$ can be determined from $\langle X \rangle$ by the relation (2.20) and is therefore not shown. The oscillations in the means are evidence of tunneling. In Fig. 11b the U-eigenphase probability distribution for the state $|P\rangle$ is shown. The state is dominated by the same odd U-eigenstate and the doubly degenerate even eigenstates which dominate the state $|F\rangle$. Hence the tunneling period for $|P\rangle$ is the same as for $|F\rangle$. The state $|P\rangle$ is dominated by a second trio of vectors, which produce a smaller but significant effect on the evolution of the state. The second trio of vectors consists of an odd state and a nearly degenerate pair of even states. The separation of the odd eigenphase from the nearly degenerate even eigenphase determines the timescale for the secondary sinusoidal modulation in $\langle X \rangle$. The classical point orbits the fixed point and the state oscillates around $U^n|F\rangle$. The mean $\langle Y \rangle$, which is not shown, oscillates around 0.5 and undergoes collapses and revivals [2] similar to that observed in the Jaynes-Cummings model [6] and in the nonlinear oscillator model [13]. In the classical model the recurrences are rapidly damped for an initial distribution centred at the periodic point [2].

The coherent state

$$|C\rangle \equiv |j=18, \theta=1.64, \varphi=1.50\rangle \tag{3.9}$$

has a mean in the chaotic region. The mean $\langle X \rangle$ is presented in Fig. 12a and tunneling is absent. Furthermore, as demonstrated by Haake et al. [2], there are recurrences in the mean for a state in the chaotic region, but the recurrences are aperiodic (in contrast to the quasiperiodic recurrences for a state in the regular region). Recurrences are not observed for the classical model for $\langle Y \rangle$. Moreover $\langle Y \rangle$ does not deviate greatly from 0.5, whereas a decay of $\langle Y \rangle$ occurs in the classical model. The U-eigenvalue distribution in Fig. 12b reveals that the state has broadband exci-

tation. The aperiodic recurrences are similar to that observed for the Jaynes-Cummings state inversion which is subjected to thermal excitation [6]. Partial rephasings of the dominate eigenvectors produce recurrences, but the aperiodic nature is due to the dominance of incommensurate eigenphases.

The discussion here has been restricted to the case that $j=18$, $\kappa=3$ and $p=\frac{\pi}{2}$. Different values of j produce different behaviour including a more complex, although coherent, tunneling. The dependency of the model on j and κ is currently being explored.

4. The effect of measurement

We now turn to a treatment of the continual measurement of J_z. Our method is similar to that used in [8]. To model a continual measurement of J_z, we consider a sequence of instantaneous imperfect measurements of accuracy Δ repeated every T seconds. The continual measurement is then defined by a limiting procedure, in which T is made small and Δ is made large such that the product ΔT is kept constant. This limiting procedure seems to reproduce results of more realistic continual measurement models where the output of the apparatus contains the signal together with added white noise [14]. In that case Δ appears as the total noise added by the apparatus while T is defined by the inverse response bandwidth of the apparatus. Our approach will be to determine the evolution of the system between kicks including continual measurement of J_z as described above. The evolution is then suspended as a kick is applied, and the evolution recommences following the kick.

The measurement is modelled by coupling the system to a set of apparatuses between kicks. This coupling is described by the Hamiltonian

$$H_{SA}=g\sum_r J_z\, Y_r\, \delta(t-rT) \tag{4.1}$$

where the sum is over as many apparatuses as are used and g is a coupling constant. The operator Y_r is one of a pair of canonically conjugate operators (X_r, Y_r) for the r^{th} apparatus such that

$$[X_r, Y_{r'}]=i\hbar\,\delta_{rr'}. \tag{4.2}$$

Simultaneous with the coupling a perfect readout of X_r is made and the result X_r is recorded. Each apparatus is used only once and discarded. In this way we model the more realistic situation in which a single apparatus is always coupled to the system, but for which correlations in the apparatus are rapidly damped. The apparatus thus contains no information on the history of the recordings.

The apparatus states are assumed to be minimum uncertainty states $|\psi_n\rangle$ with wave functions

$$\langle x_r|\psi_r\rangle=(2\pi\Delta)^{-1/2}\exp(-x_r^2/4\Delta). \tag{4.3}$$

After the interaction with the apparatus the state of the system is transformed from the state $\rho \equiv\rho_s(t)\otimes|\psi_r\rangle\langle\psi_r|$ to

$$\rho'(t)=\exp(-\mathrm{i}\,g\,J_z\,Y_r/\hbar)\,\rho(t)\exp(\mathrm{i}\,g\,J_z\,Y_r/\hbar) \tag{4.4a}$$

and the probability of obtaining a result x_r is given by

$$P(x_r,t)=\mathrm{tr}_{S,A}(\rho'(t)|x_r\rangle\langle x_r|) \tag{4.4b}$$

where we trace over both the system and the apparatus. Performing the trace over the apparatus we obtain

$$P(x_r,t)=\mathrm{tr}_s(\rho_s(t)\;\Upsilon^\dagger(x_r)\;\Upsilon(x_r)) \tag{4.5}$$

where

$$\Upsilon(x_r)=(2\pi\Delta)^{-1/4}\exp\left(-\frac{(x_r-g\,J_z)^2}{4\Delta}\right). \tag{4.6}$$

This is a distribution with mean

$$\bar{x}_r(t)=g\langle J_z(t)\rangle \tag{4.7}$$

and variance

$$(\Delta x_r(t))^2=\Delta+g^2(\Delta J_z(t))^2 \tag{4.8}$$

where the variance of J_z is

$$(\Delta J_z(t))^2=\langle(J_z(t))^2\rangle-\langle J_z(t)\rangle^2. \tag{4.9}$$

In what follows we set the amplication g to unity without loss of generality.

The parameter Δ is the resolution of the apparatus. If Δ is too large then no information is obtained regarding the system state: a readout of the physical quantity X_r simply follows the statistics of the prepared apparatus state. Conversely, when $\Delta\to 0$ we obtain a perfect readout of J_z. In this section we are interested in the large j limit. If we took this limit with Δ held fixed, we would be considering measurement models which were increasingly accurate: the relative width of the spectrum resolved by Δ is smaller and smaller. To define a fixed class of measurement models we need to scale Δ with j. We choose the scaling

$$\Delta=\sigma j \tag{4.10}$$

with σ fixed independently of j. This is expected to define a 'least disturbing' class of measurements. To

see this let us consider a system which is prepared in the lowest eigenstate of J_x. A perfect measurement of $J_z(\Delta \to 0)$ then completely destroys all the information contained in the initial preparation but, of course, maximises the information obtained regarding J_z. What we require is a Δ just large enough to resolve the statistics of J_z, but not so large as to destroy all the information in the initial state. This is achieved if Δ is roughly the variance of the J_z distribution in the initial state. Using the uncertainty relation for angular momentum this gives $\Delta \sim j$.

Equation (4.5) determines the statistics of the readout. We need now to consider how the system state changes conditioned on a particular result X_r. The new system state is given by

$$\rho'_{x_r}(t) = (P(x_r, t))^{-1}\, \Upsilon(x_r)\, \rho(t)\, \Upsilon^{\dagger}(x_r). \tag{4.11}$$

In this paper we are actually interested in the unconditional change in the system state subject to measurement. This is given by summing over all the partitions defined in (4.11):

$$\rho'(t) = \int_{-\infty}^{\infty} \mathrm{d}x_r\, \Upsilon(x_r)\, \rho(t)\, \Upsilon^{\dagger}(x_r). \tag{4.12}$$

Following reference [8] we can now obtain an evolution equation for the unconditional state between kicks. The evolution equation is

$$\frac{\mathrm{d}\rho}{\mathrm{d}t} = -i\frac{\kappa}{2j}[J_z^2, \rho] - \frac{\Gamma}{2j}[J_z, \rho]] \tag{4.13}$$

where

$$\Gamma = (4\sigma T)^{-1}. \tag{4.14}$$

The constant T is the time between successive measurements and we have taken $\sigma \to \infty$ and $T \to 0$ such that the product σT is constant. In a continual measurement model of this sort, only the product σT is significant. This measurement parameter Γ defines a particular class of measurements independent of j.

The double commutator in (4.13) completely specifies the effect of continual measurement on the system evolution between kicks. The effect of the double commutator term on the first-order moments is

$$\frac{\mathrm{d}}{\mathrm{d}t}\langle J_x\rangle = -\frac{\kappa}{2j}\langle J_z J_y + J_y J_z\rangle - \frac{\Gamma}{2j}\langle J_x\rangle \tag{4.15a}$$

and

$$\frac{\mathrm{d}}{\mathrm{d}t}\langle J_y\rangle = \frac{\kappa}{2j}\langle J_z J_x + J_x J_z\rangle - \frac{\Gamma}{2j}\langle J_y\rangle \tag{4.15b}$$

while all moments of J_z and $\mathbf{J}^2$ remain unaffected by measurements. In the semiclassical limit ($j \to \infty$) the effect of the measurement on the first-order moments vanishes. Thus we do not need to modify the classical map to take account of the continual measurement of J_z. In contrast the dissipative mechanism of Grobe and Haake [4] does modify the classical map.

An important consequence of the double commutator term appears when we consider the evolution of the off-diagonal elements in the J_z-eigenstate basis. The solution of (4.13) is

$$\rho_{nm}(t) = \exp\{-[i\kappa(n^2 - m^2) + \Gamma(n-m)^2]\, t/2j\}\, \rho_{nm}(0) \tag{4.16}$$

where $\rho_{nm}(t) \equiv \langle jn|\rho(t)|jm\rangle$. The effect of measurement is to diagonalise the system in the basis of the measured quantity J_z. In the language of measurement theory the J_z-eigenstates form the pointer basis [15].

As discussed in Sect. 3, quantum tunneling is due to the coherence between different eigenstates of the unitary evolution operator. It is thus instructive to consider the effect of measurement in the eigenstate basis of the evolution operator. Let us define the complex constant

$$\gamma^{nm} \equiv -\frac{\mathrm{d}}{\mathrm{d}t}\langle\phi_n|\rho(t)|\phi_m\rangle|_{t=0} \tag{4.17}$$

and the real part of (4.17) is the coherence damping rate. By inserting the master equation (4.13) into (4.17) we obtain the expression

$$2j\gamma^{nm} = -i\kappa\langle\phi_n|[J_z^2, \rho(0)]|\phi_m\rangle - \Gamma\langle\phi_n|[J_z, [J_z, \rho(0)]]|\phi_m\rangle. \tag{4.18}$$

As a particular example of coherence decay we consider the superposition state

$$\rho(0) = \tfrac{1}{2}(|\phi_m\rangle + |\phi_n\rangle)(\langle\phi_m| + \langle\phi_n|) \tag{4.19}$$

and the real part of the parameter γ^{nm} is given by

$$\begin{aligned}\mathrm{Re}(\gamma^{nm}) &= \frac{\Gamma}{2j}\{2\langle J_z^2\rangle - \langle\phi_n|J_z|\phi_n\rangle\langle\phi_m|J_z|\phi_m\rangle \\ &\quad -(\langle\phi_n|J_z|\phi_n\rangle + \langle\phi_m|J_z|\phi_m\rangle)\,\mathrm{Re}(\langle\phi_n|J_z|\phi_m\rangle) \\ &\quad -\mathrm{Re}(\langle\phi_n|J_z|\phi_m\rangle^2)\}\end{aligned} \tag{4.20}$$

where the mean of J_z^2 is

$$\langle J_z^2\rangle = T_r(\rho(0)J_z^2)$$
$$= \tfrac{1}{4}[\langle\phi_n|J_z^2|\phi_n\rangle + \langle\phi_m|J_z^2|\phi_m\rangle + 2\,\mathrm{Re}(\langle\phi_n|J_z^2|\phi_m\rangle)]. \quad (4.21)$$

Grobe and Haake [4] show that in a region of global chaos ($\kappa \geqq 6$) the J_z-eigenbasis matrix elements of the evolution operator eigenstate $|\phi_m\rangle$ is

$$\langle jm|\phi_n\rangle \cong (2j+1)^{-1/2}\exp(\mathrm{i}\psi_m) \quad (4.22)$$

where the ψ_m are uniformly distributed in the interval $0 \leqq \psi_m \leqq 2\pi$. The phase randomness suggests that the terms in (4.20) without phase information dominate the sum. Thus, the coherence damping rate is approximated by

$$\mathrm{Re}(\gamma^{nm}) \cong \frac{\Gamma}{4j}\{\langle\phi_n|J_z^2|\phi_n\rangle + \langle\phi_m|J_z^2|\phi_m\rangle - 2\langle\phi_n|J_z|\phi_n\rangle\langle\phi_m|J_z|\phi_m\rangle\}$$
$$= \frac{\Gamma}{4j}\sum_{k,l=-j}^{j}|\langle\phi_n|jk\rangle|^2|\langle\phi_m|jl\rangle|^2(k-l)^2. \quad (4.23)$$

Inserting expression (4.22) into (4.23) produces

$$\mathrm{Re}(\gamma^{nm}) \cong \frac{1}{6}\Gamma j\left(1+\frac{1}{j}\right) \quad (4.24)$$

which is similar to the result obtained by Grobe and Haake [4] for the dissipative model in the globally chaotic case. We see that coherence decay between eigenstates of the unitary evolution operator decay more rapidly as $j \to \infty$. Although the result is valid for $\kappa \geqq 6$ when global chaos exists in the classical regime, we expect that, for a given parameter Γ, quantum coherences will be more rapidly damped as j increases for $\kappa < 6$ also.

In (4.23) it is apparent that damping is greatest when the distribution $|\langle jm|\phi_n\rangle|^2$ has broad support on m; in that case large values contribute to the sum. This is indeed the case in the chaotic region ($\kappa \geqq 6$) where the distribution is uniform. In the regular region ($\kappa \leqq 2$) $|\langle\phi_n|jk\rangle|^2$ is more narrowly supported on k and we thus expect the sum (4.23) to be smaller. This leads us to conjecture that measurement-induced coherence decay will proceed more rapidly in chaotic systems than in regular systems. This requires further investigation.

The effect of measurement on quantum tunneling is particularly interesting as it provides a good example of the quantum Zeno effect. It has been suggested for some time that a system with a discrete spectrum which is subjected to continual observation will have

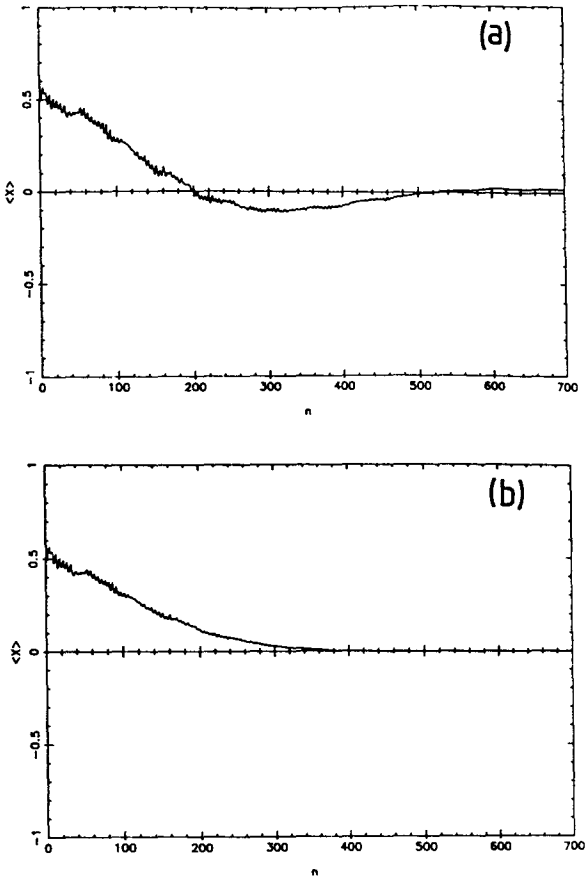

Fig. 13a and b. The quantum mean $\langle X\rangle$ for the initial coherent state $|F\rangle$ for **a** $\Gamma = 0.00072$ and **b** $\Gamma = 0.00144$

dynamics quite different from free evolution. In the extreme case of arbitrarily accurate, instantaneous measurements, the free dynamics can be entirely frozen [9].

In [9] a two-level system is subjected to continual observation and the effects on the Rabi oscillations between the two levels are analysed. When the measurement parameter Γ exceeds the Rabi frequency, the rate of change of the system from the initial state decreases as Γ increases. That is, the Rabi oscillations are overdamped. The oscillation in a two-level system is an approximation to the tunneling in a bistable well. The overdamping of Rabi oscillations and of tunneling in the bistable well are dynamical manifestations of the quantum Zeno effect.

Exactly the same behaviour is evident in the tunneling between fixed points for the kicked nonlinear top considered here. In Fig. 13 we consider the fixed point tunneling for $j = 18$ in the underdamped regime ($\Gamma = 0.00072$) and near critical damping ($\Gamma = 0.00144$). Thus, the tunneling oscillations are damped by the effects of measurement. If no measurement occurs then the state has tunneled to the other fixed point

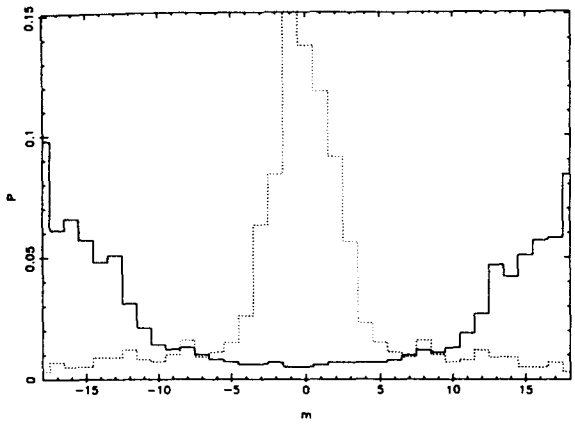

Fig. 14. The $J_{\|}$ (solid line) and $J_{\perp}$ (dashed line) eigenvalue distribution for the state $|F\rangle$ at the time 300τ for $\Gamma = 0.00144$

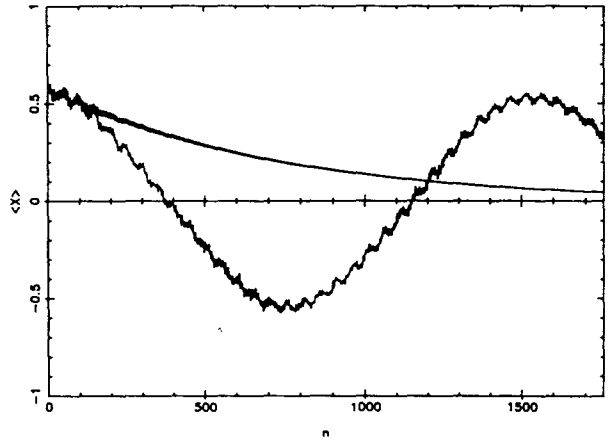

Fig. 15. The quantum mean $\langle X\rangle$ for the initial coherent state $|j=35, \theta=2.25, \varphi=0.63\rangle$ which has a mean at a fixed point, for $\Gamma=0$ (solid line) and $\Gamma=0.00072$ (dashed line)

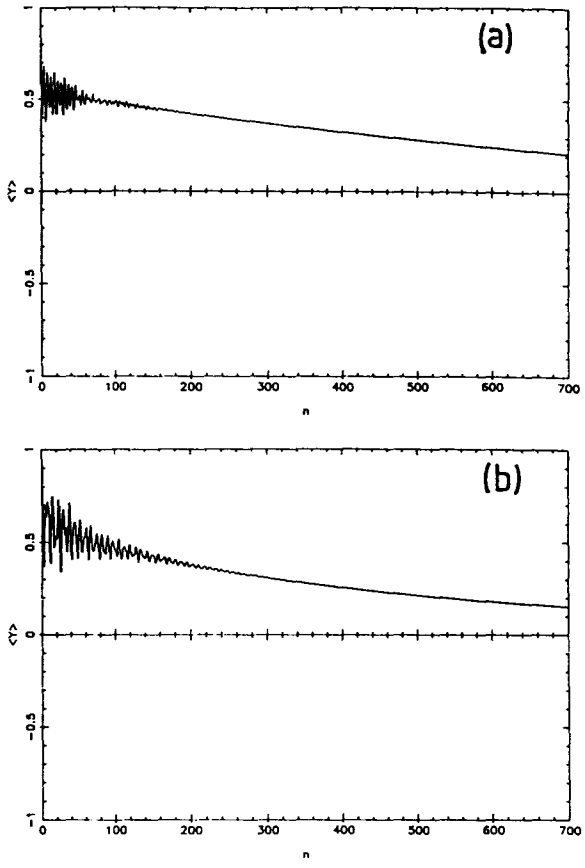

Fig. 16a and b. The quantum mean $\langle Y\rangle$ for the initial states **a** $|P\rangle$ and **b** $|C\rangle$ for $\Gamma=0.0036$ and $j=18$

at $n=300$, as seen in Fig. 7. However, in Fig. 14, we observe that, for Γ chosen at the critical damping level the state is now localized at the two fixed points in the $J_{\|}$ eigenvalue distribution. Interference fringes are not present in the $J_{\perp}$ eigenvalue distribution: the coherence which is a signature of a superposition state has been destroyed and the state at $n=300$ is now similar to a mixture of the coherent states at the fixed points. The coherence has been destroyed and the dynamics is essentially frozen. Measurement destroys the coherences between the dominant odd state and the pair of dominant even eigenstates. The decay of coherence between the even and odd states determines the damping time of the oscillations in Fig. 13.

In Fig. 15 the effect of measurement on tunneling is presented. We observe that coherent tunneling between the fixed points for $j=35$ is similar to the tunneling which occurs for $j=18$. For some values of j the tunneling oscillations are complicated by additional dominant eigenphases, but here we choose the relatively simple cases of $j=18$ and $j=35$ to illustrate the semiclassical limit of measurement. However, when continual measurement is incorporated into the dynamics and the measurement parameter $\Gamma=0.00072$ (which corresponds to the underdamped tunneling case for $j=18$), overdamping occurs for $j=35$. As we expect, the Zeno effect acts to suppress the quantum tunneling in the semiclassical limit ($j\to\infty$). Grobe and Haake [4] observe a similar phenomenon: the two-cycle tunneling is damped in the dissipative model.

Measurement destroys the coherent tunneling which is a quantum feature of the dynamics. The other important quantum feature, recurrences, is also affected by continual measurement. The recurrences of the means for an initial distribution in the classical kicked nonlinear top are rapidly damped. The recurrences of the *quantum* means, however, continue ad infinitum, but the inclusion of a continual J_z-measurement into the dynamics damps the recurrences in both the regular region (Fig. 16a) and the

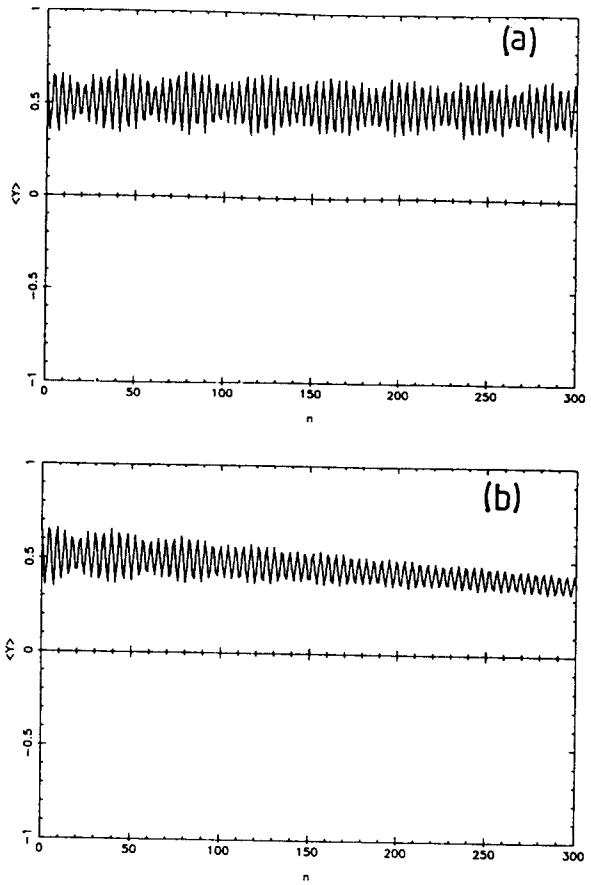

Fig. 17a and b. The quantum mean $\langle Y \rangle$ for the state $|j=35, \theta=2.10, \varphi=0.94\rangle$ which has a mean at a periodic point, for **a** $\Gamma=0$ and **b** $\Gamma=0.0036$

chaotic region (Fig. 16b). Moreover, for $\Gamma=0.0036$, which damps the recurrences in the regular region prior to the first revival, the recurrences in the regular and chaotic regions are damped over the same time scale.

The damping of coherent tunneling is interpreted as a destruction of the coherences between the dominant odd state and the even eigenstate pair for the coherent state with a mean at the fixed point. The rapid decay of tunneling is readily observed. However, the analysis of quantum recurrences and measurement-induced coherence decay is more complicated. Quantum recurrences are a consequence of the coherences of a multitude of vectors. As we observed in Fig. 16, measurement destroys the recurrences.

In the semiclassical limit we expect that all pairwise damping constants will be very large from (4.24). However the semiclassical limit is difficult to illustrate by comparing cases for two different j values as the eigenphase spectrum and the damping constants are very sensitive to the value of j. In Fig. 17a we observe the behaviour of $\langle Y \rangle$ for the initial coherent state with a mean in the periodic region of phase space. The oscillations resemble collapses and revivals, but a complete dephasing, which is necessary for a collapse, does not occur. Whereas for $j=18$ collapses occur, the eigenphase spacing for $j=35$ prevents complete collapses from occurring. Nevertheless the inclusion of continual measurement destroys the recurrences as shown in Fig. 17b except for a persistent oscillatory component which eventually damps out. The persistence is a consequence of a small damping constant for that particular coherence. It is difficult to observe if recurrences are damped more rapidly by comparing Figs. 16 and 17, due to the complicated dependence of the eigenphase spectrum and the coherence damping rates on j for $\kappa=3$, but we expect all coherence decays to become very rapid in the large j limit. We are investigating the j-dependence of recurrences and of damping rates and we will present our results in a future publication.

5. Conclusions

The quantisation of the kicked nonlinear top dynamics, which are classically chaotic, results in such nonclassical features as coherent tunneling between fixed points and recurrences in the means. A continual measurement scheme which provides a 'least disturbing' class of measurements has been incorporated into the dynamics. The classical dynamics are unchanged by the continual measurement, but, in the semiclassical limit, coherent tunneling is suppressed and recurrences in the mean are expected to be suppressed also. Continual measurement of the quantum system acts to suppress the quantum feature.

We have concentrated on the cases where $j=18$ and $j=35$ which provide relatively simple behaviour, but a careful analysis of the j-dependence of the model is essential. We are currently pursuing this analysis. Furthermore, coherences between the U-eigenvectors are destroyed by the act of measurement. A better understanding of the destruction of the coherences, and the effects on tunneling and recurrences, would be obtained by computing the pairwise damping constants for the U-eigenvectors.

BCS would like to acknowledge useful discussions with P. Byrom. This work has been supported by the Australian Research Council.

References

1. Frahm, H., Mikeska, H.J.: Z. Phys. B – Condensed Matter **60**, 117 (1985)
2. a) Haake, F., Kuś, M., Scharf, R.: Z. Phys. B – Condensed Matter **65**, 381 (1987);

b) Haake, F., Kuś, M., Mostowski, J., Scharf, R.: In: Coherence, cooperation, and fluctuations. Haake, F., Nauducci, L., Walls, D. (eds.), p. 200. New York: Cambridge University Press 1986
3. Kuś, M., Scharf, R., Haake, F.: Z. Phys. B – Condensed Matter **66**, 129 (1987)
4. a) Grobe, R., Haake, F.: Lecture Notes in Physics. Vol. **282**, 267. Berlin, Heidelberg, New York: Springer 1987;
b) Grobe, R., Haake, F.: Z. Phys. B – Condensed Matter **68**, 503 (1987)
5. Grobe, R., Haake, F., Sommers, H.-J.: Phys. Rev. Lett. **61**, 1899 (1988)
6. a) Milburn, G.J.: Opt. Acta **31**, 671 (1984);
b) Barnett, S.M., Knight, P.L.: Phys. A **33**, 2444 (1986);
c) Puri, R.R., Agarwal, G.S.: Phys. Rev. A **33**, 3610 (1986)
7. Barchielli, A.: Phys. Rev. D **32**, 347 (1985)
8. Caves, C.M., Milburn, G.J.: Phys. Rev. A **36**, 5543 (1987)
9. Milburn, G.J.: J. Opt. Soc. Am. B **5**, 1317 (1988)
10. Sanders, B.C.: Phys. Rev. A **40**, 2417 (1989)
11. a) Arrechi, F.T., Courtens, E., Gilmore, R., Thomas, H.: Phys. Rev. A **36**, 5543 (1987);
b) Perelomov, A.: Generalized coherent states and their applications. Berlin: Springer 1986
12. a) Caldeira, A.O., Leggett, A.J.: Ann. Phys. **149**, 374 (1983);
b) Razavy, M., Pimpale, A.: Phys. Rep. **168**, 305 (1988)
13. Milburn, G.J.: Phys. Rev. A **33**, 674 (1986)
14. Milburn, G.J.: Phys. Rev. A **36**, 5271 (1987)
15. a) Zurek, W.H.: Phys. Rev. D **24**, 1516 (1981);
b) Zurek, W.H.: Phys. Rev. D **26**, 1862 (1982)

B.C. Sanders, G.J. Milburn
Department of Physics
University of Queensland
St. Lucia, Queensland 4067
Australia